UAV-based Ultra High-Resolution Geodetic Mass Change Estimations near Schirmacher Oasis in East Antarctica: Insights from Sub-Seasonal, Seasonal and Annual Timescales

Ajay Godara, PJ Navinkumar, Tirthankar Ghosh, RAAJ Ramsankaran

Supplementary Information

Table S1: Geodetic mass change contribution (both in cm.w.e. and percentage) and category-wise area coverage for different slope categories for Sub-seasonal 1, Sub-seasonal 2, Seasonal and Annual periods. The Geodetic Mass Change values in the last row indicate the total Geodetic Mass Change for the given period.

Slope class	Sub-seasonal 1			Sub-seasonal 2			Seasonal			Annual		
	Geodetic Mass Change (cm.w.e.)	Geodetic Mass Change contribution	Percentage Class Area Coverage	Geodetic Mass Change (cm.w.e.)	Geodetic Mass Change contribution	Percentage Class Area Coverage	Geodetic Mass Change (cm.w.e.)	Geodetic Mass Change contribution	Percentage Class Area Coverage	Geodetic Mass Change (cm.w.e.)	Geodetic Mass Change contribution	Percentage Class Area Coverage
0-2°	0.06	5.20%	26.95%	-0.15	12.40%	23.97%	-0.126	37.50%	26.45%	0.178	8.60%	28.35%
2-5°	0.81	66.50%	47.68%	-0.52	43.10%	47.19%	-0.112	33.30%	48.18%	0.671	32.40%	46.86%
5-10°	-0.31	25.70%	24.53%	0.39	32.10%	27.63%	0.094	27.80%	24.78%	1.159	55.90%	24.17%
10-20°	-0.03	2.60%	0.84%	0.15	12.00%	1.19%	0.005	1.40%	0.59%	0.067	3.20%	0.62%
>20°	0	0	0	0.01	0.40%	0.02%	0	0	0	0	0	0
	0.53			**-0.14**			**-0.14**			**2.07**		

Table S2: Geodetic mass change contribution (both in cm.w.e. and percentage) and aspect-wise area coverage for different aspect class for Sub-seasonal 1, Sub-seasonal 2, Seasonal and Annual periods. The Geodetic Mass Change values in the last row indicate the total Geodetic Mass Change for the given period.

Aspect class	Sub-seasonal 1			Sub-seasonal 2			Seasonal			Annual		
	Geodetic Mass Change (cm.w.e.)	Geodetic Mass Change contribution	Percentage Class Area Coverage	Geodetic Mass Change (cm.w.e.)	Geodetic Mass Change contribution	Percentage Class Area Coverage	Geodetic Mass Change (cm.w.e.)	Geodetic Mass Change contribution	Percentage Class Area Coverage	Geodetic Mass Change (cm.w.e.)	Geodetic Mass Change contribution	Percentage Class Area Coverage
N	-0.34	22.40%	54.06%	0.64	31.70%	50.39%	0.16	20.70%	55.00%	2.27	66.00%	55.95%
NE	0.77	51.00%	20.47%	-0.64	31.70%	17.99%	-0.28	36.20%	18.13%	-0.41	12.00%	19.17%
E	0.23	15.60%	6.18%	-0.30	14.70%	7.17%	-0.12	15.20%	6.38%	-0.23	6.70%	6.22%
NW	-0.13	8.60%	10.13%	0.28	13.80%	12.45%	0.13	17.20%	10.73%	0.38	11.10%	9.74%
SE	0.01	1.00%	3.03%	-0.10	4.70%	3.99%	-0.04	5.60%	3.14%	-0.04	1.10%	2.76%
S	0.00	0.20%	2.06%	-0.03	1.60%	2.61%	-0.02	2.10%	2.28%	0.00	0.10%	2.15%
SW	0.00	0.30%	1.59%	-0.01	0.50%	2.11%	0.00	0.10%	1.75%	0.03	0.90%	1.67%
W	-0.01	0.90%	2.48%	0.02	1.20%	3.29%	0.02	3.00%	2.58%	0.07	2.00%	2.35%
	0.53			**-0.14**			**-0.14**			**2.07**		

S1: Surface Elevation, Slope and Aspect:

The slope, aspect, and surface elevation contours for the surveyed dates are presented in this section. Figure S1(a-f) shows the spatially distributed slope and aspect with surface elevation contours at every 10m interval for 17 Nov 23, 03 Dec 23 and 17 Dec 23 covering the smaller area. This smaller area depicts the summer period (Fig. 1, red outline). Figure *S2* (a-d) shows the spatially distributed slope and aspect with same elevation contours of 10m interval for 03 Dec 23 and 21 November 24 depicting the annual period (Fig. 1, black outline).

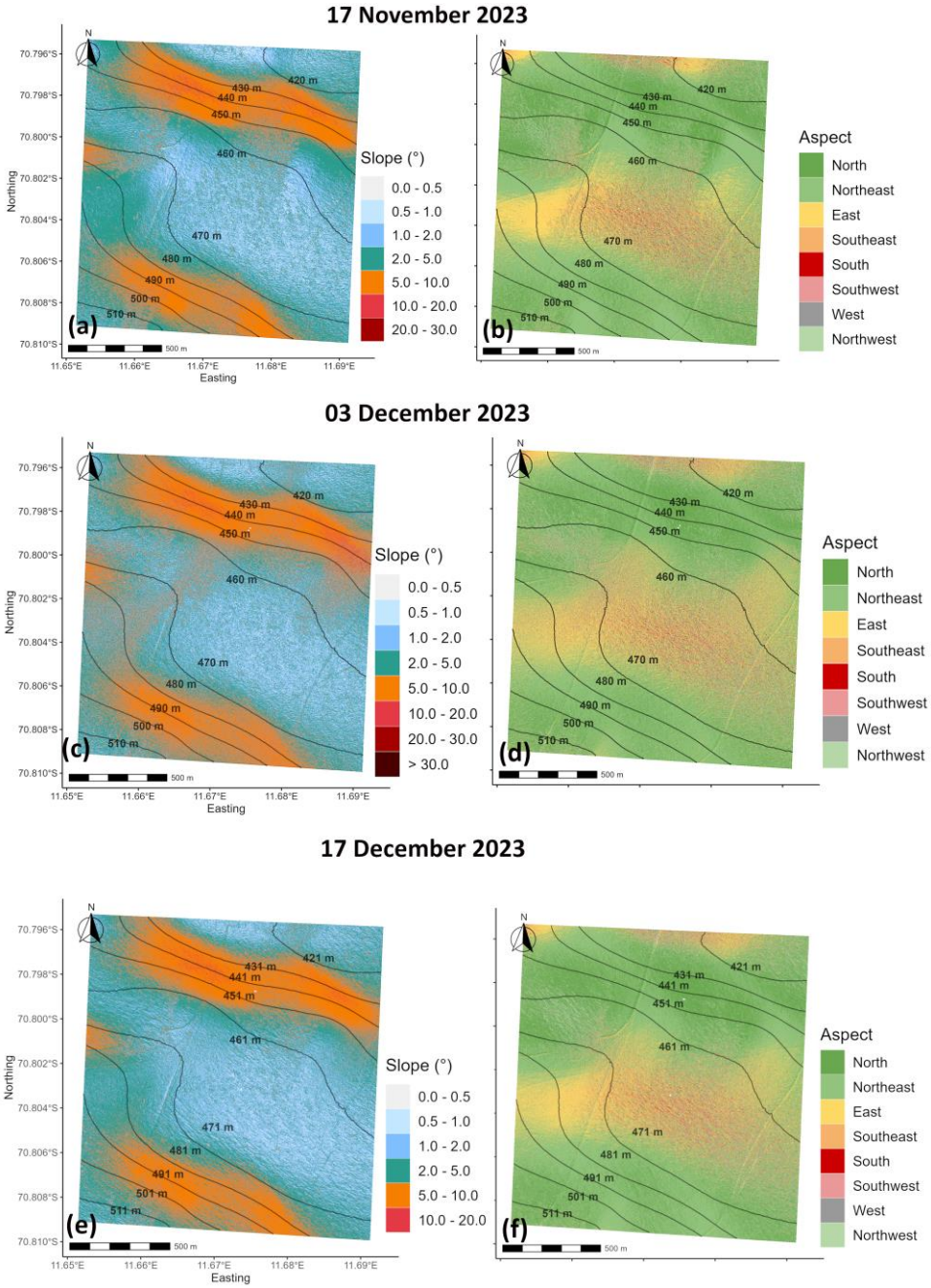

Figure S1: Spatially distributed slope and aspect maps during summer period on 17 November 2023 (a), (b); 03 December 2023 (c), d), and 17 December 2023 (e), f)

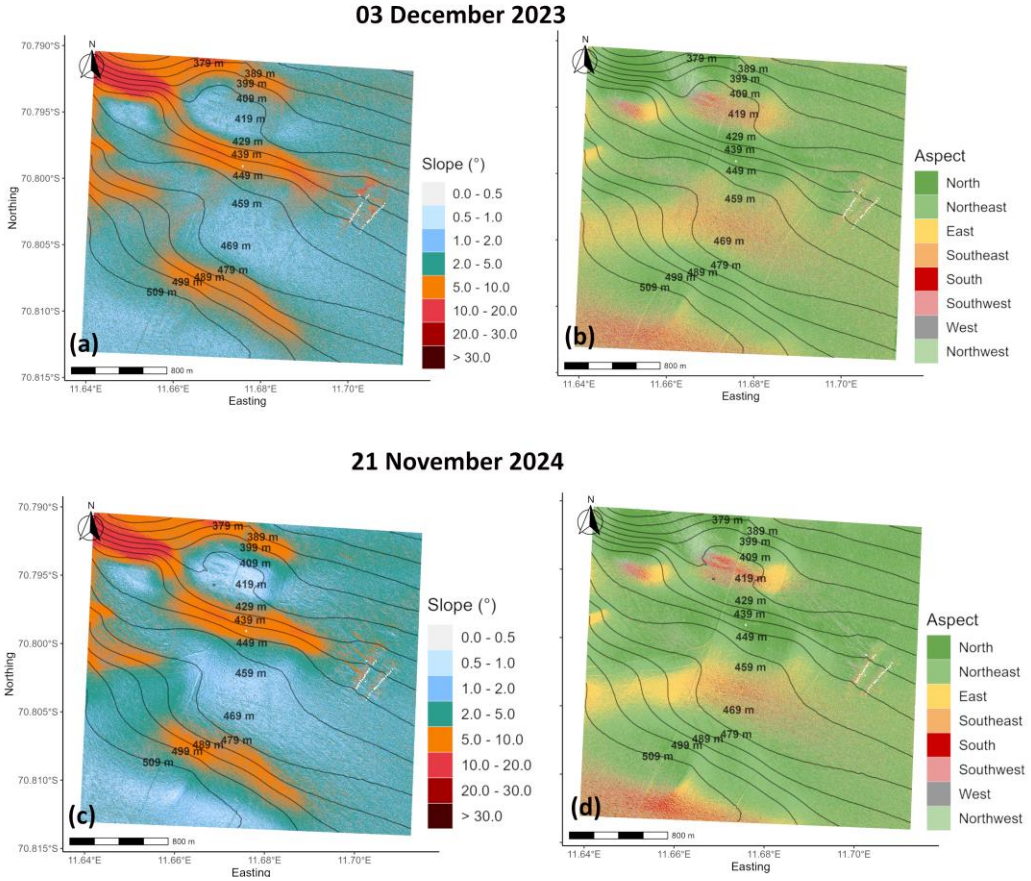

Figure S2: Spatially distributed slope and aspect maps on 03 December 2023 (a), (b), and 21 November 2024 (c), d). These maps are generated from UAV DEMs of the corresponding dates. The coverage area is for the larger footprint.

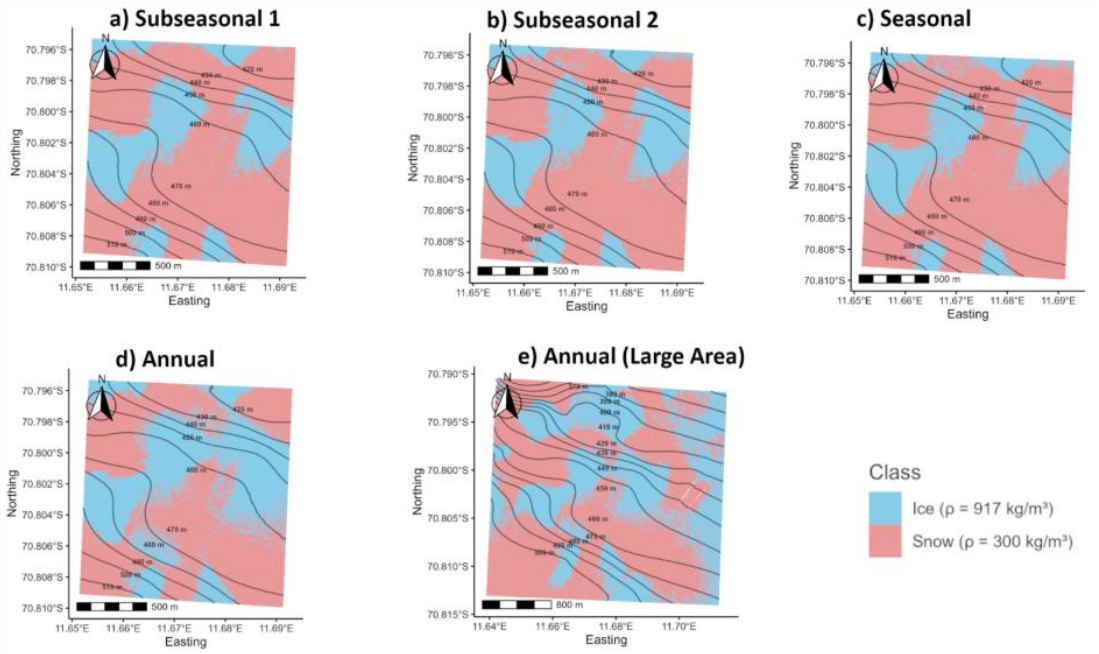

Figure S3: The spatial distribution map of snow and ice cover in the UAV surveyed area for a) Sub seasonal-1; b) Sub seasonal-2; c) Seasonal and d) Annual (same as seasonal study area), and e) Annual (large area). It represents the transition and evolution of the surface characteristics with time. In the figure, blue represents the ice and pink represents the snow.

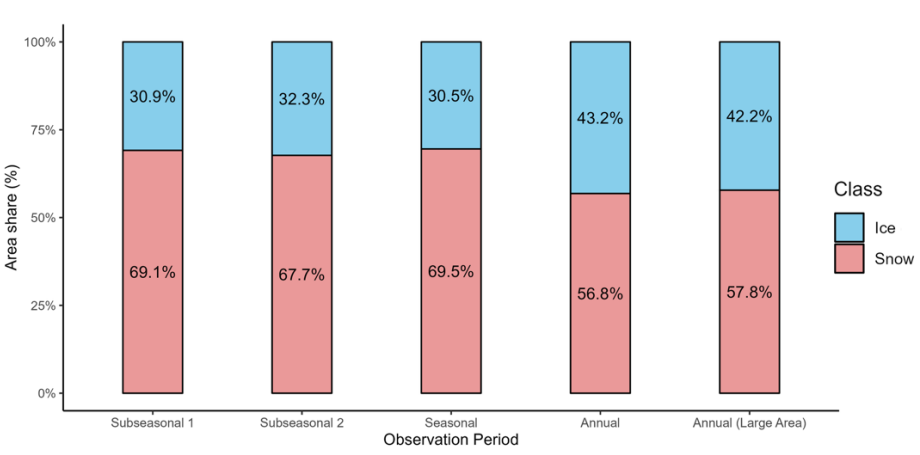

Figure S4: The stacked histogram plot shows the snow and ice cover area (in %) for different periods in the UAV surveyed area.

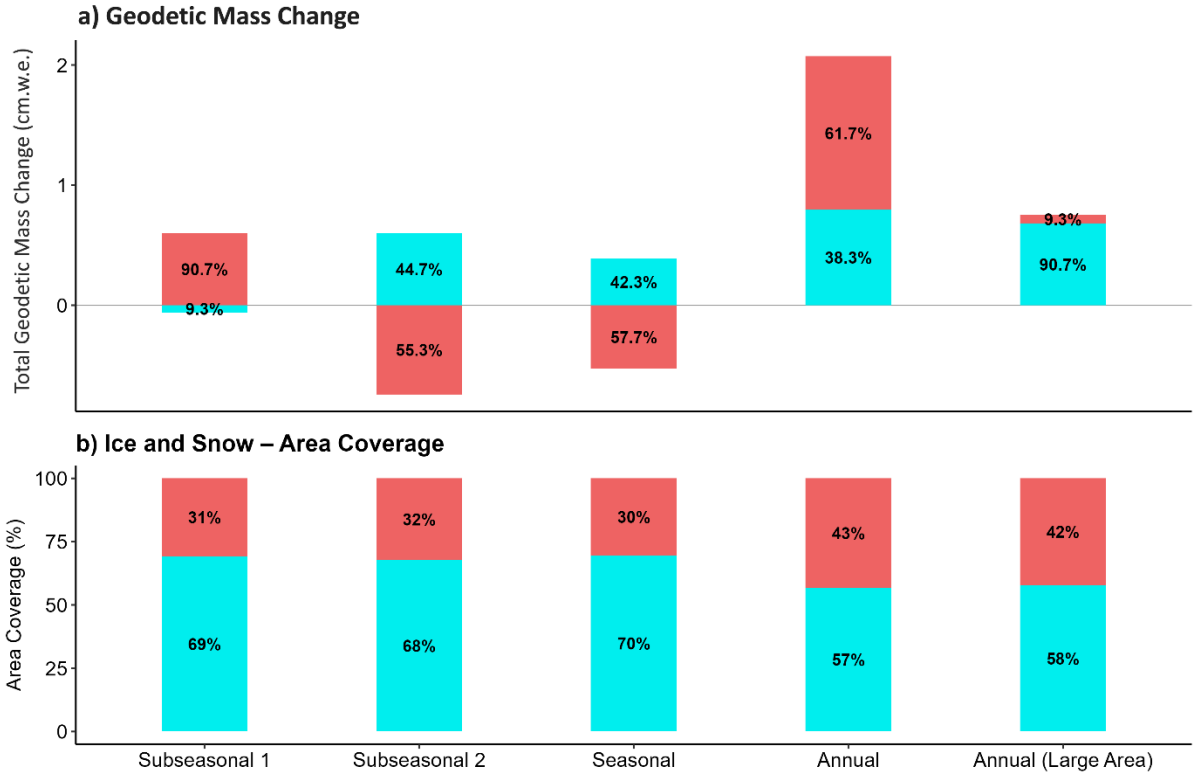

Figure S5. (a) Stacked bars showing the total Geodetic Mass Change (in cm w.e.) for each observation period. Ice (red) and Snow (blue) components indicate their contributions to total Geodetic Mass Change, with percentage values inside each bar denoting their relative share of Geodetic Mass Change magnitude. (b) Corresponding fractional area coverage of snow and ice during the same periods. Red bars represent ice-covered surfaces, and blue bars represent snow-covered surfaces.

S2. Comparison of in-situ Mass Change and UAV-derived Geodetic Mass Change

This section compares the UAV-derived geodetic mass change with interpolated in situ stake-based measurements from annual scale. Typically, point observations at stake locations are interpolated and used to validate or calibrate satellite-derived geodetic mass change estimates at larger scales. However, the 1.5 km spacing and interpolation of stake data may not adequately capture local-scale variations within that distance. Therefore, this analysis evaluates how interpolated field-based geodetic mass change estimates differ from the UAV-derived one.

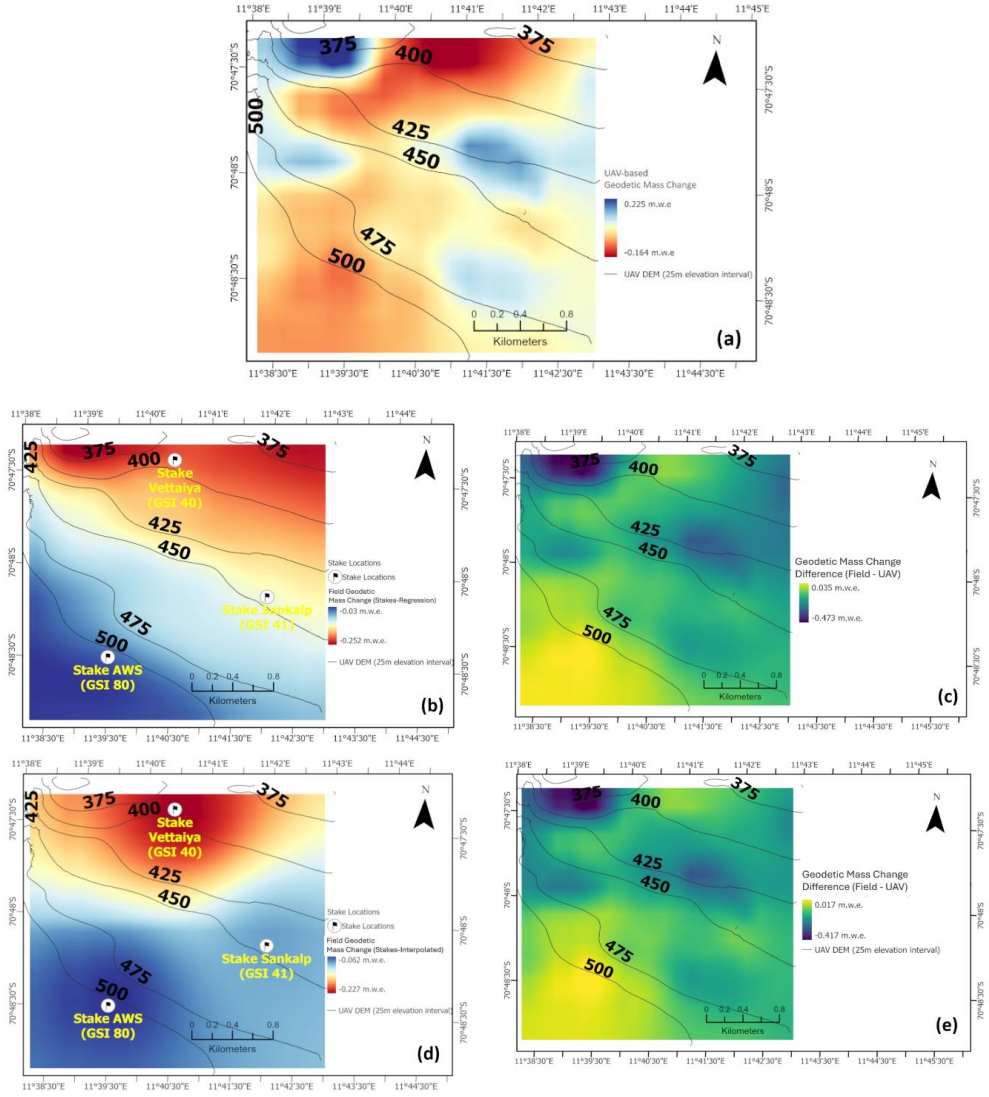

Figure S6: Map of spatially distributed annual geodetic mass change estimates at Annual scale from (a) UAV-based. (b) Stake-based geodetic mass change obtained using regression, (c) Difference between UAV-based and regression-based geodetic mass change. (d) Stake-based geodetic mass change obtained using inverse distance weighting (IDW) interpolation. (e) Difference between UAV-based and IDW-based geodetic mass change. Here, elevation contours represent 25 m intervals (in black lines), and stake locations (AWS, Vettaiya, Sankalp) are indicated by flag symbol.

The UAV-based geodetic mass change estimates (Fig. S6a) reveal strong spatial heterogeneity across the surveyed area, with more negative geodetic mass change in the north and less negative values toward the

south. Although the regression-based method captures the broad elevation dependence of geodetic mass change**,** it does not reproduce the spatial heterogeneity resolved by the UAV data. The difference map (Fig. S6c) shows deviations ranging from −0.473 to +0.035 m w.e. The IDW-interpolated stake geodetic mass change (Fig. S6d), constrained by only three stake locations, produces spatial patterns that diverge from the UAV-based geodetic mass change results. The corresponding difference map (Fig. S6e) shows systematic mismatches of −0.417 to +0.017 m w.e. Together, the difference between the interpolated geodetic mass change estimates and UAV-based estimates (Figures S6c and S6e) indicate that both approaches yield spatially inconsistent results and fail to capture the local variability as observed by the UAV.

References

Miller, B. B. and Carter, C.: The test article, J. Sci. Res., 12, 135–147, doi:10.1234/56789, 2015.

Smith, A. A., Carter, C., and Miller, B. B.: More test articles, J. Adv. Res., 35, 13–28, doi:10.2345/67890, 2014.